High-field magnetotransport in a two-dimensional electron gas in quantizing magnetic fields and intense terahertz laser fields

2004 J. Phys.: Condens. Matter 16 89

(http://iopscience.iop.org/0953-8984/16/1/009)

INSTITUTE OF PHYSICS PUBLISHING JOURNAL OF PHYSICS: CONDENSED MATTER

J. Phys.: Condens. Matter **16** (2004) 89–101 PII: S0953-8984(04)63781-7

High-field magnetotransport in a two-dimensional electron gas in quantizing magnetic fields and intense terahertz laser fields

W Xu[1], R A Lewis[2], P M Koenraad[3] and C J G M Langerak[4]

[1] Department of Theoretical Physics, Research School of Physical Sciences and Engineering, Australian National University, Canberra, ACT 0200, Australia
[2] Institute for Superconducting and Electronic Materials, University of Wollongong, Wollongong, NSW 2522, Australia
[3] COBRA Inter-University Research Institute, Eindhoven University of Technology, PO Box 513, 5600 MB Eindhoven, The Netherlands
[4] FOM Institute Rijnhuizen, NL-3430 BE Nieuwegein, The Netherlands

E-mail: wen105@rsphysse.anu.edu.au

Received 22 May 2003
Published 15 December 2003
Online at stacks.iop.org/JPhysCM/16/89 (DOI: 10.1088/0953-8984/16/1/009)

Abstract

We present a combined experimental and theoretical study of interactions between two-dimensional electron gases (2DEGs) and terahertz (THz) free-electron lasers in the presence of quantizing magnetic fields. It is found both experimentally and theoretically that when an intense THz field and a quantizing magnetic field are applied simultaneously to a GaAs-based 2DEG in the Faraday geometry, a strong cyclotron resonance (CR) effect on top of the magnetophonon resonances can be observed by *transport* measurements at relatively *high temperatures*. With increasing radiation intensity and/or decreasing temperature, the peaks of the CR are broadened and split due to magnetophoton–phonon scattering.

1. Introduction

Measurement of photoconductivity in a semiconductor-based two-dimensional electron gas (2DEG) in the presence of a magnetic field is a powerful tool in studying important phenomena such as cyclotron resonance (CR) [1]. In recent years, low-temperature photoconductivity in GaAs-based 2DEG systems in quantizing magnetic fields has been investigated intensively [2–5]. In these experimental works, such devices as far-infrared (FIR) spectrometers, p-Ge lasers, B-field-modified light emission from n-InSb, etc, were applied as the FIR or terahertz (10^{12} Hz or THz) radiation sources. These measurements have been used to study quantum Hall effects and to realize important devices such as quantum Hall far-infrared (QHFIR) detectors. On the other hand, the recent application of long-wavelength free-electron laser (FEL) radiation

to the investigation of electronic, transport and optical properties of semiconductor-based electron gas systems [6, 7] has opened up a new field of research in the interactions between electrons and intense laser fields in semiconductor devices. The current generation of FELs has already provided a tunable source of linearly polarized intense laser radiation in the THz bandwidth [8]. More interestingly, a very recently achieved experimental set-up has made it possible to perform measurements in different semiconductor devices under FEL radiation in the presence of high magnetic fields.

When an electronic system (e.g. a 2DEG) is subjected simultaneously to THz radiation and to quantizing magnetic fields, we enter a regime with different competing energies, such as the electron kinetic energy, electronic subband separation, Fermi energy, cyclotron energy, photon energy, plasmon energy and phonon energy. These energies (frequencies) are of the order of microelectronvolts (THz), which implies that intense THz radiation fields can couple strongly to the semiconductors and modify strongly the processes of momentum and energy excitation and relaxation of electrons in the systems. Thus, by using a FEL as an intense THz radiation source, we are able to examine how an intense radiation field affects the fundamental magnetotransport and magnetooptical properties of, for example, 2DEGs.

At present, in the investigation of semiconductor-based 2DEG systems using THz FELs in the presence of magnetic fields, most of the published results are obtained from optical measurements [7]. In this work, we use a rather straightforward experimental set-up to measure the *magnetotransport* properties of a GaAs/AlGaAs heterojunction subjected simultaneously to THz FEL radiation and quantizing magnetic fields in the Faraday geometry. The experimental results are presented in section 2. In section 3, we develop a tractable theory to understand and reproduce our experimental findings. Further discussion of the theoretical and experimental results is presented in section 4 and the conclusions obtained from this study are summarized in section 5.

2. Experiments and experimental results

In this work, we use FELIX (Free Electron Laser for Infrared eXperiments, The Netherlands) for the experimental investigation of an $Al_{0.3}Ga_{0.7}As/GaAs$ heterojunction in the presence of quantizing magnetic fields. The sample was grown by MBE at about 650 K with modulation-doping (Si: 1.33×10^{18} m^{-3}). It has eight contacts (conventional Hall bar): two current contacts and six contacts on the sides of the sample. The distance between two adjacent contacts is 500 μm and the distance between two opposite contacts is 260 μm. The zero-field and low-temperature electron density and mobility of this sample are found to be 2×10^{11} cm^{-2} and 200 m^2 V^{-1} s^{-1}, respectively. During the measurements, the top of the sample is covered with a metal mask with a small hole in the middle. This hole is placed just above the Hall bar to ensure that the laser illuminates only the 2DEG and not the contacts. Furthermore, a black polyethylene filter may be placed above the sample to block ambient light.

In the absence of the FEL irradiation (light-off), the Shubnikov–de Haas oscillations (SdHo), quantum Hall effects (QHE) and magneto-phonon resonances (MPR) are clearly observed in this sample. These phenomena at light-off are well known and, therefore, in this paper, we will focus on the results obtained in the presence of the FEL fields. The measurements are carried out in the following configuration:

(1) the growth direction of the 2DEG is taken along the z axis and, therefore, the 2DEG is formed in the xy plane;
(2) the static magnetic field B is applied along the z direction; and

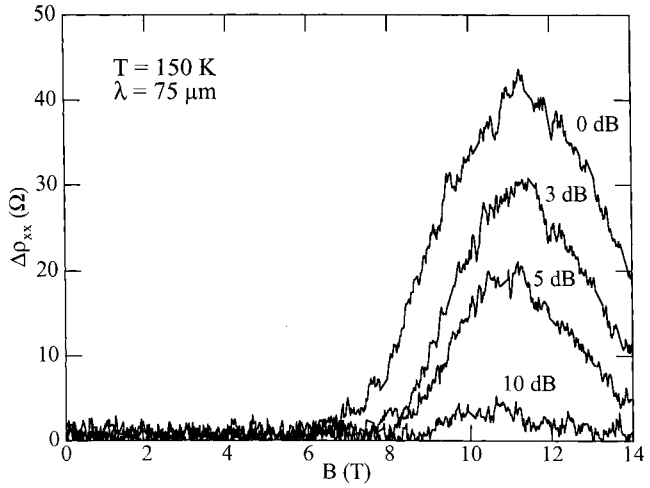

Figure 1. The difference in ρ_{xx} between light-on and light-off as a function of magnetic field at a fixed radiation wavelength ($\lambda = 75$ μm, which corresponds to $f = \omega/2\pi = 4$ THz) for different radiation intensities. The radiation intensity is altered through optical attenuation (i.e. 0 dB corresponds to a radiation without attenuation).

(3) the FEL field with a vector potential $A(t)$ is applied parallel to the B field and polarized linearly in the 2D plane (taken to be along the x direction).

In this configuration (known as the Faraday geometry for a 2DEG), the magnetic and radiation fields do not couple to the confining potential of the 2DEG; however, the magnetic field couples directly to the radiation field. As a result, the effect of the CR can be observed when the radiation frequency ω approaches the cyclotron frequency ω_c. By a simple transport measurement, i.e. applying a dc current along the x direction and measuring the voltage along this direction as well, we can examine the dependence of transport coefficients on magnetic and radiation fields.

It is well known that, at relatively high temperatures and in the absence of a radiation field, when the longitudinal resistivity ρ_{xx} is measured as a function of magnetic field in a GaAs-based 2DEG, we can observe a series of oscillations described as the magnetophonon resonance (MPR) effect [9]. This occurs whenever the energy separation between two Landau levels equals the energy of the longitudinal optic (LO) phonon. When switching on the FEL radiation, we find that, on top of the MPR effect, we can also observe a strong CR effect when $\omega \sim \omega_c$. In figure 1, the difference in ρ_{xx} between light-on and light-off ($\Delta\rho_{xx}$) at a temperature $T = 150$ K is shown as a function of magnetic field at a fixed radiation frequency for different radiation intensities. It should be noted that the MPR oscillations are observed in the light-off and light-on data of ρ_{xx}, but do not appear appreciably in the difference. From our experimental data, we find that, in the presence of intense laser radiation, the CR effect is far stronger than the MPR effect in ρ_{xx} and the strength of the CR increases with radiation intensity. When the radiation frequency is away from the cyclotron frequency, the effect of the radiation is weak. The most significant experimental result we draw from figure 1 is that, in the presence of the intense THz laser radiation, we can observe a strong CR effect at relatively high temperatures, even through simple transport measurements. We know that, in the past, the most popular way to observe the CR effect is through optical and/or photoresistivity measurements carried out at very low temperatures ($T \sim 1$ K) [1–5, 10] through necessity to satisfy $\omega\tau \gg 1$.

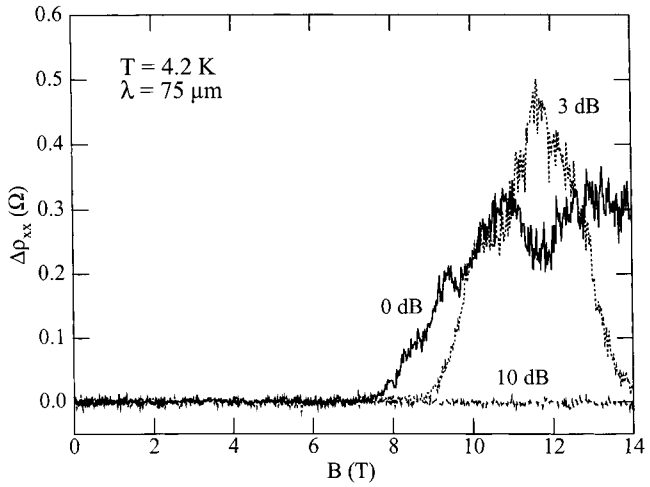

Figure 2. The difference in ρ_{xx} between laser light-on and light-off at a fixed radiation frequency for different radiation intensities at a relatively low temperature. In these measurements, a polyethylene filter to block ambient light was removed to obtain a higher FEL radiation level compared to figure 1. Similar features can be observed up to $T \sim 150$ K.

Another interesting experimental result is that, at relatively low temperatures ($T < 150$ K), the CR is split into two peaks when rather high-intensity FEL radiation is applied in the Faraday geometry. In figure 2 we show the difference in ρ_{xx} between light-on and light-off at $T = 4.2$ K as a function of magnetic field at a fixed radiation frequency for different radiation intensities, which confirms that the splitting is due to the intense radiation. We note that, under the FELIX irradiation, the similar phenomenon to that shown in figure 2 can be observed up to $T \sim 150$ K and the effect is more pronounced at a lower temperature. The $\Delta\rho_{xx}$ shown in figure 2 is much smaller than that shown in figure 1 on account of the different temperature of the two measurements. It should be pointed out that the splitting of the CR peak observed in our experiments has some features essentially different to those measured in [2–5].

(1) In contrast to those low-temperature results shown in [2–5], under the FELIX irradiation, the splitting can be observed up to $T \sim 150$ K, although a more pronounced splitting can been seen at relatively low temperatures.
(2) In [2–5], the splitting of the CR peaks at low temperatures is due to the presence of the relatively large dc currents applied to the sample, whereas in our experiments the splitting is induced mainly by intense laser fields, as shown in figure 2.
(3) Most importantly, the splitting of the CR peaks measured in [2–5] occurs only at even-integer filling factors $\nu = hn_e/eB$ (e.g. at $\nu = 2$ or 4), whereas the effect observed in our experiments can be seen over a wide B-field regime as long as the condition for CR is satisfied.

From the low-T and light-off data of the total electron density $n_e = 2 \times 10^{11}$ cm^{-2}, which corresponds to $\nu = 1$ at $B = 8.27$ T, the CR in figures 1 and 2 occurs at $B > 10$ T—a regime of $\nu < 1$ where the CR effect depends very little on the filling factor.

From figures 1 and 2 we see that there is a significant shift of the cyclotron frequency to the higher magnetic field regime under intense THz radiation. This implies such radiation enhances the electron effective mass. When a 2DEG is subjected to intense radiation fields, there are two contributions to the higher-than-usual electron effective mass. The first is the

temperature dependence, which can lead to an increase of about 0.005 m_e, with m_e being the rest electron mass, due to stronger electronic screening. This effect has been discussed and verified experimentally [11]. The second and more important contribution comes from the increase in the electron energy under intense laser radiation. Around the cyclotron frequency, electrons can gain energy quickly from the radiation field via the CR effect and move into the increasingly non-parabolic regime of the conduction band. Thus, a further enhancement of electron effective mass can be expected. From our experimental data, we estimate that the energy gained for an electron in the CR condition is about 220 meV, which is reasonable under the radiation condition provided by FELIX. Moreover, unlike the filling factor, which is independent of the electron effective mass m^*, the cyclotron frequency $\omega_c = eB/m^*$ depends on m^*. We note that one normally takes m^* as that obtained at the bottom of the conduction band. The results shown in figures 1 and 2 indicate that, in the presence of intense THz laser radiation and quantizing magnetic fields, the CR effect in a GaAs-based 2DEG depends more strongly on the electron effective mass than the filling factor.

In order to understand experimental findings detailed above, we present below a tractable theoretical approach to study the influence of intense laser radiation on the transport and optical properties of a 2DEG in the presence of a quantizing magnetic field.

3. Theoretical results

It can be shown that, when a magnetic field and an electromagnetic (EM) field are included within the electron Hamiltonian for a 2DEG in the Faraday geometry, the Landau gauge and Coulomb gauge can correctly describe the magnetic field and EM field, respectively. Including the laser field within the Coulomb gauge and the magnetic field within the Landau gauge, the electron Hamiltonian for a 2DEG subjected to a magnetic field B (applied along the z direction) and a laser field $A(t)$ (polarized linearly along the x direction) can be written, in the absence of scattering centres, as

$$H_0(t) = \frac{1}{2m^*}[(p_x - eA(t))^2 + (p_y + eBx)^2 + p_z^2] + U(z), \tag{1}$$

where $p_x = -i\hbar\partial/\partial x$ is the momentum operator along the x direction, m^* is the effective electron mass, $A(t) = A_0 \sin(\omega t)$ is the vector potential induced by the EM field polarized along the x direction, ω is the radiation frequency, $A_0 = F_0/\omega$, with F_0 being the electric field strength of the EM field and $U(z)$ is the confining potential energy of the 2DEG along the growth direction. The time-dependent Schrödinger equation: $i\hbar\partial\Psi(\mathbf{R}, t)/\partial t = H_0(t)\Psi(\mathbf{R}, t)$, can be solved analytically [12] where $\mathbf{R} = (x, y, z)$. With the time-dependent electron wavefunction we can derive the retarded Green function for electrons in the $(\mathbf{R}, t)$ representation:

$$G_0(\mathbf{R}, t; \mathbf{R}', t') = \frac{\Theta(t - t')}{i\hbar} \sum_{N,k_y,n} \Psi^*_{N,k_y,n}(\mathbf{R}', t')\Psi_{N,k_y,n}(\mathbf{R}, t), \tag{2}$$

which satisfies $[i\hbar\partial/\partial t - H_0(t)]G_0(\mathbf{R}, t; \mathbf{R}', t') = \delta(\mathbf{R} - \mathbf{R}')\delta(t - t')$. Here, N is the Landau level index, n is the index for the nth electronic subband and k_y is the electron wavevector along the y direction. Applying the Green function approach to the time-dependent perturbation theory, it can be shown that, in the presence of a scattering potential $V(\mathbf{R}, t)$, the first-order contribution to the steady-state electronic transition rate can be calculated by (see the appendix)

$$W_{\alpha'\alpha} = \frac{1}{\hbar^2} \lim_{t-t'\to+\infty} \frac{\partial[G^*_{\alpha'\alpha}(t, t')G_{\alpha'\alpha}(t, t')]}{\partial(t - t')}, \tag{3}$$

where $G_{\alpha'\alpha}(t, t') = \int_{t'}^{t} d\tau \, \langle\alpha', \tau|V(\mathbf{R}, \tau)|\alpha, \tau\rangle$, with $|\alpha, t\rangle$ being the time-dependent electron wavefunction.

For the case of electron–phonon coupling, the interaction Hamiltonian is

$$V(\mathbf{R},t)=\sum_{\mathbf{Q}}[V_{\mathbf{Q}}a_{\mathbf{Q}}\mathrm{e}^{\mathrm{i}(\mathbf{Q}\cdot\mathbf{R}+\omega_Q t)}+V_{\mathbf{Q}}^{*}a_{\mathbf{Q}}^{\dagger}\mathrm{e}^{-\mathrm{i}(\mathbf{Q}\cdot\mathbf{R}+\omega_Q t)}], \tag{4}$$

where $\mathbf{Q}=(\mathbf{q},q_z)=(q_x,q_y,q_z)$ is the phonon wavevector, ω_Q is the phonon frequency, $(a_{\mathbf{Q}}^{\dagger},a_{\mathbf{Q}})$ are the canonical conjugate coordinates of the phonon system and $V_{\mathbf{Q}}$ is the electron–phonon coupling coefficient. After introducing the time-dependent electron wavefunction [12] and scattering potential for electron–phonon coupling (equation (4)) into equation (3), the first-order contribution to the steady-state electronic transition rate induced by magnetophoton–phonon scattering in a 2DEG is obtained as

$$W_{N'N,n'n}=\sum_{m_1,m_2=-\infty}^{\infty}W_{N'N,n'n}^{(m_1,m_2)}, \tag{5a}$$

where $m_1(m_2)$ refers to emission and absorption of photons (magnetons) and the contributions from different optical and magnetic processes are

$$W_{N'N,n'n}^{(m_1,m_2)}=\frac{2\pi}{\hbar}\sum_{\mathbf{Q}}\left[N_Q+\frac{1}{2}\mp\frac{1}{2}\right]|V_{\mathbf{Q}}|^2G_{n'n}(q_z)C_{N',N}(l^2q^2/2)J_{m_2}^2(r_0q)$$
$$\times J_{m_1}^2\left[r_0\sqrt{q_x^2+(\omega_{\mathrm{c}}q_y/\omega)^2}\right]\delta(E_{N'}-E_N+\varepsilon_{n'}-\varepsilon_n-m_1\hbar\omega+m_2\hbar\omega_{\mathrm{c}}\mp\hbar\omega_Q). \tag{5b}$$

Here, the upper (lower) case refers to absorption (emission) of a phonon with an energy $\hbar\omega_Q$, $N_Q=(\mathrm{e}^{\hbar\omega_Q/k_{\mathrm{B}}T}-1)^{-1}$ is the phonon occupation number, $G_{n'n}(q_z)=|\langle n'|\mathrm{e}^{\mathrm{i}q_z z}|n\rangle|^2$ is the form factor for the electron–phonon interaction along the growth direction, with $|n\rangle$ being the electron wavefunction along this direction, $C_{N,N+J}(x)=[N!/(N+J)!]\mathrm{e}^{-x}x^J[L_N^J(x)]^2$ is induced by the electron interaction with the magnetic field, with $L_N^J(x)$ being the associated Laguerre polynomials, $J_m(x)$ is a Bessel function and $r_0=(eF_0)/[m^*(\omega^2-\omega_{\mathrm{c}}^2)]$. Moreover, in the above derivations, the effect of the Zeeman spin splitting has been neglected because here we are only interested in cyclotron resonance observed at relatively high temperatures, which is independent of the spin degeneracy and the filling factor.

When a 2DEG interacts with the magnetic and radiation fields in the presence of a scattering centre, the electronic transitions are accompanied by emission and absorption of photons and magnetons. As can be seen from equation (5), the total electronic transition rate is the summation over all possible optical and magnetic processes including multi-photon and multi-magneton channels. For the case of a high-frequency ($\omega\gg1$) and/or low-intensity ($F_0\ll1$) radiation, such that $r_0\ll1$, the electronic transition rate given by equation (5) becomes the one obtained by using Fermi's golden rule derived in the absence of a radiation field. Because of the coupling between the magnetic and radiation fields, the CR effect can be seen in the magnetophoton–phonon interactions via the factor r_0. Furthermore, we note that, as in the case where the radiation field is not applied, the presence of a quantizing magnetic field leads to a singularity of the electronic transition rate. This singular nature is characterized by a δ function which reflects the fact that energy is conserved during a scattering event.

Using the following properties of a δ function: (1) $\delta(a-b)=\int_{-\infty}^{\infty}\mathrm{d}E\,\delta(E-a)\delta(E-b)$; (2) $\delta(x)=(2\pi)^{-1}\int_{-\infty}^{\infty}\mathrm{d}y\,\mathrm{e}^{\mathrm{i}xy}$; and (3) $\delta(E)\to(\Gamma/\pi)/(E^2+\Gamma^2)$, with Γ being the width of the broadened scattering states, we find that the contribution from different optical and magnetic channels to the transition rate induced by magnetophoton–phonon coupling can be summed up and the total transition rate is given by

$$W_{N'N,n'n}=\frac{8}{\hbar^2\omega}\sum_{\mathbf{Q}}\left[N_Q+\frac{1}{2}\mp\frac{1}{2}\right]|V_{\mathbf{Q}}|^2G_{n'n}(q_z)C_{N',N}(l^2q^2/2)\int_0^{\infty}\mathrm{d}x\,\cos(2\nu^{\pm}x)$$

$$\times \mathrm{e}^{-2x\Gamma/\hbar\omega} J_0[2r_0 q \sin(x\omega_\mathrm{c}/\omega)] J_0\Big[2r_0\sqrt{q_x^2 + (\omega_\mathrm{c} q_y/\omega)^2}\sin x\Big], \tag{6}$$

with $\nu^{\mp} = (E_{N'} - E_N + \varepsilon_{n'} - \varepsilon_n \mp \hbar\omega_Q)/\hbar\omega$.

From the electronic transition rate, one can evaluate the electronic scattering rate or relaxation time. The statistically averaged electronic scattering rate (or inverse of the relaxation time) induced by the magnetophoton–phonon interaction in a 2DEG system is

$$1/\tau = \sum_{N',N,n',n} f(E_N + \varepsilon_n)[1 - f(E_{N'} + \varepsilon_{n'})] W_{N'N,n'n} \Big/ \sum_{N,n} f(E_N + \varepsilon_n), \tag{7}$$

with $f(E)$ being the electron energy-distribution function. Using the electronic scattering rate or relaxation time, the magnetoresistivities can be calculated by, for example, the Drude model:

$$\rho_{xx} = \frac{m^*}{n_\mathrm{e} e^2}\frac{1}{\tau} \qquad \text{and} \qquad \rho_{xy} = \frac{B}{n_\mathrm{e} e} \tag{8}$$

where n_e is the total electron density of the 2DEG. Thus, we can calculate the magnetotransport coefficients induced by electron–phonon scattering in the presence of laser and magnetic fields in the Faraday geometry.

4. Further discussions

It should be noted that the photon energy of THz radiation ($\hbar\omega \sim$ meV) is much less than the energy gaps ($E_\mathrm{g} \sim$ eV) among different bands and valleys in semiconductor materials such as GaAs. Therefore, the effect of interband and intervalley transitions through corresponding optical mechanisms can be neglected. As a consequence, the electron–photon–phonon scattering becomes the limiting factor in determining the transport and optical properties in semiconductor-based 2DEGs driven by intense THz fields. For polar semiconductors such as GaAs, the frequency of the phonon oscillation associated with LO modes is at the THz level so that the electron–LO-phonon coupling is the principal channel for relaxation of THz-excited electrons in a GaAs-based 2DEG. A strong electron–LO-phonon scattering in the sample used in the measurements has been evident by the observation of the MPR effect in ρ_{xx}. Hence, in the present theoretical study, we only consider electron interactions with LO phonons. For electron–LO-phonon scattering: (i) $\omega_Q \simeq \omega_\mathrm{LO}$, the LO-phonon frequency in the long-wavelength range; (ii) $N_Q \simeq N_0 = (\mathrm{e}^{\hbar\omega_\mathrm{LO}/k_\mathrm{B}T} - 1)^{-1}$; and (iii) the coupling coefficient is given by the Fröhlich Hamiltonian: $|V_\mathbf{Q}|^2 = 4\pi\alpha L_0(\hbar\omega_\mathrm{LO})^2/Q^2$, where α is the electron–LO-phonon coupling constant and $L_0 = (\hbar/2m^*\omega_\mathrm{LO})^{1/2}$ is the polar radius. In the present theoretical work, our calculations are conducted for the AlGaAs/GaAs heterojunction sample used experimentally. The sample and material parameters are:

(1) the effective electron mass at the bottom of the conduction band $m^* = 0.0665\, m_\mathrm{e}$, where m_e is the rest electron mass;
(2) the total electron density $n_\mathrm{e} = 2 \times 10^{11}$ cm^{-2};
(3) the electron mobility at low temperatures and zero-magnetic field $\mu_0 = 200$ m^2 V^{-1} s^{-1};
(4) the LO-phonon energy $\hbar\omega_\mathrm{LO} = 36.6$ meV; and
(5) the electron–LO-phonon coupling constant $\alpha = 0.068$.

Furthermore, we consider the situation where only the lowest electronic subband is occupied by electrons in the heterojunction and apply the usual triangular well approximation to model the confining potential normal to the interface of the heterojunction [13] so that the form factor $G_{00}(q_z)$ can be determined analytically.

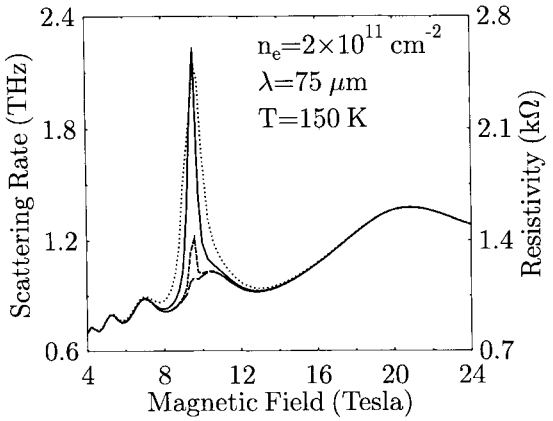

Figure 3. Magnetophoton–phonon scattering rate and longitudinal resistivity as a function of magnetic field at a fixed radiation wavelength for different radiation intensities up to $F_0 = 2$ kV cm^{-1}. The long-dashed, broken, full and dotted curves are, respectively, for radiation intensities $F_0 = 0.1$, 0.3, 1 and 2 kV cm^{-1}.

Since most of our measurements are carried out at relatively high temperatures and high radiation levels, we use a Maxwellian distribution as the statistical energy distribution function for electrons through $f(E) = c\mathrm{e}^{-E/k_\mathrm{B}T}$, where the normalization factor c is determined by the condition of electron number conservation. To our knowledge, at present, little is known about how an intense radiation field affects the broadening of the scattering states. Here we assume that the width of the broadened scattering states, Γ, is proportional to the width of the Landau levels, γ, so that $\Gamma = a\gamma$. In the calculations, we use results obtained from the self-consistent Born approximation for the Landau level width and take $a = 20$. Under the short-range scattering approximation, we have [13] $\gamma = \hbar\omega_\mathrm{c}[2/(\pi\mu_0 B)]^{1/2}$, where the mobility $\mu_0 = 200$ m^2 V^{-1} s^{-1} is taken from the experimental data.

In figure 3, the scattering rate of magnetophoton–phonon coupling and the longitudinal resistivity ρ_{xx} are shown as a function of magnetic field at a fixed radiation frequency for different intensities[5]. The magnetophonon resonances can be seen at $B \simeq 5$, 7, 11, 21 T (where $\omega_\mathrm{LO} \sim \beta\omega_\mathrm{c}$ with $\beta = 4$, 3, 2, 1) when the radiation frequency is away from the cyclotron frequency. A strong effect of the radiation can be seen when $\omega_\mathrm{c} \sim \omega$, where:

(1) the CR effect can be observed, which can be much more pronounced than the MPR effect at high intensity radiation;
(2) the strength of the CR increases with increasing radiation intensity up to $F_0 = 2$ kV cm^{-1} at $T = 150$ K; and
(3) when higher-intensity radiation is applied, the peak of the CR is broadened. These results are in line with those observed experimentally (see figure 1).

The magnetophoton–phonon scattering rate and ρ_{xx} as a function of magnetic field are shown in figure 4 at a fixed radiation frequency for different high radiation intensities. We find that, at $T = 150$ K and when $F_0 > 2$ kV cm^{-1}, a splitting of the peak of the CR is observed theoretically and the splitting increases with increasing radiation intensity.

From the theoretical results shown above, we can understand the physical reason behind what we have seen experimentally. For relatively low intensity radiation and when $\omega \sim \omega_\mathrm{c}$,

[5] The connection between the electric field strength of a laser field (F_0) and the laser output power (P) in the vacuum is $P = 0.5\sqrt{\epsilon/\mu}|F_0|^2 \simeq 1.32|F_0|^2$ kW cm^{-2}, where F_0 is in units of kV cm^{-1}.

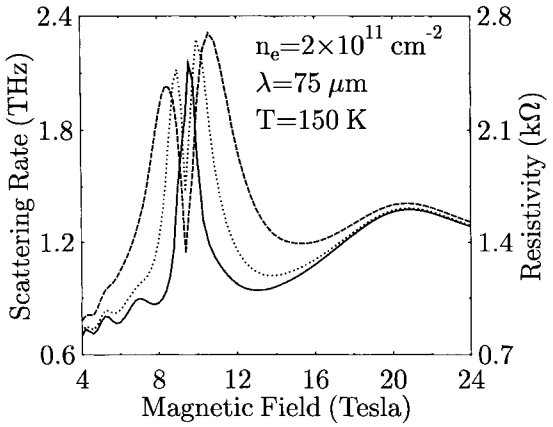

Figure 4. Magnetophoton–phonon scattering rate and longitudinal resistivity as a function of magnetic field at a fixed radiation wavelength for different radiation intensities when $F_0 \geqslant 2$ kV cm^{-1}. The full, dotted and broken curves are, respectively, for radiation intensities $F_0 = 2$, 5 and 10 kV cm^{-1}.

electrons in the system can gain energy efficiently from the radiation field via the CR effect and lose the energy through the emission of phonons. This two-step process opens up new channels for electronic transitions and, as a result, the scattering rate and resistivity increase with increasing radiation intensity. When the radiation intensity is strong enough so that electrons can gain energy from the radiation field much more quickly than they lose it by the emission of phonons, the electronic transition events are mainly achieved through cyclotron resonance. In this case, the effective electron–phonon scattering is suppressed and the magnetophoton–phonon scattering rate, along with ρ_{xx}, decreases with increasing radiation intensity. As a consequence, the splitting of the peak of the CR can be observed at high intensity radiation fields when $\omega \sim \omega_c$. Therefore, the splitting of the CR that we see experimentally is mainly due to electron interactions with the radiation fields and scattering centres. Moreover, a lower temperature results in a weaker electron–phonon coupling because of a smaller phonon occupation number. This implies that the splitting of the CR can be more easily detected at relatively low temperatures. It is interesting to mention that recently a similar splitting of the CR has also been observed experimentally in SiC-based structures [14]. In these recent experiments, optically detected cyclotron resonance (ODCR) was measured as a function of relatively low magnetic field (large filling factors) at a fixed microwave radiation frequency for different radiation powers. The splitting of the CR is clearly seen when the radiation power is larger than 100 mW at $T = 1.6$ K for SiC. In that work, the authors also attributed the splitting of the CR effect to electron–phonon interactions.

From figures 3 and 4, we note that, in the presence of intense THz radiation, the rate for electronic scattering in a GaAs-based 2DEG via magnetophoton–phonon interaction is of the order of the THz radiation frequency (i.e. $\omega\tau \sim 1$). This suggests that the intense THz radiation can modify strongly the processes of momentum and energy excitation and relaxation of electrons in the system in the presence of quantizing magnetic fields, and this is the main reason why a strong influence of the radiation field on magnetotransport coefficients can be observed experimentally. The tractable theoretical approach developed here can reproduce qualitatively the results obtained experimentally and can be used to understand those fundamentally new experimental findings. It should be noted that, in the theoretical results presented, the parameter r_0 diverges when $\omega_c \sim \omega$. This is mainly because, in the model, we only consider an ideal

situation with features such as a 'pure' radiation frequency and a 'strict' linear polarization of the radiation field. For real radiation sources, e.g. FELs, the radiation frequency is slightly broadened and the linear polarization of the radiation may be imperfect. Such effects dampen the singular nature of r_0 when $\omega_c \sim \omega$.

5. Conclusions

In this work, we have found experimentally that, when a GaAs-based 2DEG system is subjected simultaneously to intense THz laser fields and to quantizing magnetic fields, strong cyclotron resonance (CR) on top of the magnetophonon resonances can be observed simply by conventional magnetotransport measurements, carried out at relatively high temperatures. The strength of the CR increases with increasing radiation intensity and the effect of the radiation on ρ_{xx} becomes weak when the radiation frequency is away from the cyclotron frequency. For the case of intense THz radiation, the peak of the CR observed in ρ_{xx} is split into two and this effect is more pronounced at a lower temperature. The features of the split CR peaks under FEL irradiation are different from those reported in [2–5]. Our theoretical results indicate that these interesting radiation phenomena are mainly induced by magnetophoton–phonon scattering in the 2DEG system.

We have demonstrated that, for GaAs-based 2DEGs, strong magnetooptical effects can be observed when the magnetic field $B \sim 10$ T, the radiation frequency $f \sim 1$ THz and the radiation intensity $F_0 \sim 1$ kV cm^{-1}. These radiation conditions have been realized by the current generation of THz FELs. We believe that now it has become possible to study magnetotransport and magnetooptical properties of semiconductor-based electron gas systems in the presence of intense THz laser radiation and we expect that more interesting and important experimental and theoretical results from this research field will arise in the near future.

Acknowledgments

One of us (WX) is a Research Fellow of the Australian Research Council. We gratefully acknowledge the support of the Stichting voor Fundamenteel Onderzoek der Materie (FOM) in providing the required beam time on FELIX and highly appreciate the skillful assistance by the FELIX staff, in particular Dr AFG Van der Meer.

Appendix

In this appendix, on the basis of a time-dependent perturbation theory [15], we present a general approach to calculate the steady-state electronic transition probability in a $(\mathbf{R}, t)$ or (space, time) representation. In the absence of a scattering centre, if $|\alpha, t\rangle = \Psi_\alpha(\mathbf{R}, t)$ is the solution of the time-dependent Schrödinger equation

$$[\mathrm{i}\hbar\partial/\partial t - H_0(t)]\Psi_\alpha(\mathbf{R}, t) = 0, \tag{A.1}$$

with α being the quantum number, the retarded Green function $G_0(\mathbf{R}, t; \mathbf{R}', t')$ and the transformation function $U_0(\mathbf{R}, t; \mathbf{R}', t')$ can be determined from

$$G_0(\mathbf{R}, t; \mathbf{R}', t') = \frac{\Theta(t - t')}{\mathrm{i}\hbar} U_0(\mathbf{R}, t; \mathbf{R}', t') \tag{A.2a}$$

and

$$U_0(\mathbf{R}, t; \mathbf{R}', t') = \sum_\alpha \Psi_\alpha^*(\mathbf{R}', t')\Psi_\alpha(\mathbf{R}, t). \tag{A.2b}$$

The Green function and the transformation function satisfy, respectively,

$$[\mathrm{i}\hbar\partial/\partial t - H_0(t)]G_0(\mathbf{R}, t; \mathbf{R}', t') = \delta(\mathbf{R} - \mathbf{R}')\delta(t - t') \tag{A.3a}$$

and

$$[\mathrm{i}\hbar\partial/\partial t - H_0(t)]U_0(\mathbf{R}, t; \mathbf{R}', t') = \delta(\mathbf{R} - \mathbf{R}'). \tag{A.3b}$$

Moreover, the transformation function has features such as

$$U_0(\mathbf{R}, t'; \mathbf{R}', t') = \delta(\mathbf{R} - \mathbf{R}'), \tag{A.4a}$$

$$\Psi_\alpha(\mathbf{R}, t) = \int \mathrm{d}^3\mathbf{R}'\, U_0(\mathbf{R}, t; \mathbf{R}', t')\Psi_\alpha(\mathbf{R}', t'), \tag{A.4b}$$

$$\int \mathrm{d}^3\mathbf{R}\, U_0^*(\mathbf{R}, t; \mathbf{R}', t')U_0(\mathbf{R}, t; \mathbf{R}', t') = \int \mathrm{d}^3\mathbf{R}'\, U_0^*(\mathbf{R}, t; \mathbf{R}', t')U_0(\mathbf{R}, t; \mathbf{R}', t') = 1, \tag{A.4c}$$

and

$$\int \mathrm{d}^3\mathbf{R}_1\, U_0^*(\mathbf{R}, t; \mathbf{R}_1, t_1)U_0(\mathbf{R}_1, t_1; \mathbf{R}', t') = U_0(\mathbf{R}, t; \mathbf{R}', t'). \tag{A.4d}$$

When a scattering potential $V(\mathbf{R}, t)$ is present, the Green function $G(\mathbf{R}, t; \mathbf{R}', t')$ and the transformation function $U(\mathbf{R}, t; \mathbf{R}', t')$ should satisfy

$$G(\mathbf{R}, t; \mathbf{R}', t') = \frac{\Theta(t - t')}{\mathrm{i}\hbar}U(\mathbf{R}, t; \mathbf{R}', t'), \tag{A.5a}$$

$$[\mathrm{i}\hbar\partial/\partial t - H_0(t) - V(\mathbf{R}, t)]G(\mathbf{R}, t; \mathbf{R}', t') = \delta(\mathbf{R} - \mathbf{R}')\delta(t - t'), \tag{A.5b}$$

and

$$[\mathrm{i}\hbar\partial/\partial t - H_0(t) - V(\mathbf{R}, t)]U(\mathbf{R}, t; \mathbf{R}', t') = \delta(\mathbf{R} - \mathbf{R}'), \tag{A.5c}$$

and the transformation function should have features similar to equation (A.4). Hence, $U(\mathbf{R}, t; \mathbf{R}', t')$ can be obtained from $G(\mathbf{R}, t; \mathbf{R}', t')$ which can be determined by Dyson's equation [16] in the $(\mathbf{R}, t)$ representation:

$$G(\mathbf{R}, t; \mathbf{R}', t') = G_0(\mathbf{R}, t; \mathbf{R}', t') + \int \mathrm{d}^3\mathbf{R}_1\, \mathrm{d}t_1\, G(\mathbf{R}, t; \mathbf{R}_1, t_1)V(\mathbf{R}_1, t_1)G_0(\mathbf{R}_1, t_1; \mathbf{R}', t'). \tag{A.6}$$

The integral equation given by equation (A.6) can be solved by using an iterative approach, which is as follows:

$$G(\mathbf{R}, t; \mathbf{R}', t') = \frac{\Theta(t - t')}{\mathrm{i}\hbar}\sum_{n=0}^{\infty} U_n(\mathbf{R}, t; \mathbf{R}', t'), \tag{A.7a}$$

where U_0 is given by equation (A.2b):

$$U_1 = \frac{1}{\mathrm{i}\hbar}\sum_{\alpha,\alpha'} \Psi_{\alpha'}^*(\mathbf{R}', t')\Psi_\alpha(\mathbf{R}, t)G_{\alpha\alpha'}(t, t'), \tag{A.7b}$$

$$U_2 = \frac{1}{(\mathrm{i}\hbar)^2}\sum_{\alpha,\alpha_1,\alpha'} \Psi_{\alpha'}^*(\mathbf{R}', t')\Psi_\alpha(\mathbf{R}, t)G_{\alpha\alpha_1}(t, t')G_{\alpha_1\alpha'}(t, t'), \tag{A.7c}$$

and

$$U_n = \frac{1}{(\mathrm{i}\hbar)^n}\sum_{\alpha,\alpha_1,\ldots,\alpha_{n-1},\alpha'} \Psi_{\alpha'}^*(\mathbf{R}', t')\Psi_\alpha(\mathbf{R}, t)G_{\alpha\alpha_1}(t, t')G_{\alpha_1\alpha_2}(t, t')\cdots G_{\alpha_{n-1}\alpha'}(t, t'). \tag{A.7d}$$

Here

$$G_{\alpha'\alpha}(t, t') = \int_{t'}^{t} \mathrm{d}\tau\, \langle\alpha', \tau|V(\mathbf{R}, \tau)|\alpha, \tau\rangle. \tag{A.7e}$$

Thus, in the presence of a scattering centre, the transformation function is obtained as

$$U(\mathbf{R}, t; \mathbf{R}', t') = \sum_{n=0}^{\infty} U_n(\mathbf{R}, t; \mathbf{R}', t'). \tag{A.8}$$

From the transformation function, the averaged probability amplitude for an electronic transition from an initial state α at time t to a final state α' at time t' is obtained as

$$P_{\alpha'\alpha}(t, t') = \int \mathrm{d}^3\mathbf{R}\, \Psi^*_{\alpha}(\mathbf{R}, t) \int \mathrm{d}^3\mathbf{R}'\, \Psi_{\alpha'}(\mathbf{R}', t') U(\mathbf{R}, t; \mathbf{R}', t') = 1 + \sum_{n=1}^{\infty} P^{(n)}_{\alpha'\alpha}(t, t'), \tag{A.9a}$$

where

$$P^{(1)}_{\alpha'\alpha}(t, t') = \frac{G_{\alpha'\alpha}(t, t')}{\mathrm{i}\hbar}, \tag{A.9b}$$

$$P^{(2)}_{\alpha'\alpha}(t, t') = \frac{1}{(\mathrm{i}\hbar)^2} \sum_{\alpha_1} G_{\alpha'\alpha_1}(t, t') G_{\alpha_1\alpha}(t, t'), \tag{A.9c}$$

and

$$P^{(n)}_{\alpha'\alpha}(t, t') = \frac{1}{(\mathrm{i}\hbar)^n} \sum_{\alpha_1, \alpha_2, \ldots, \alpha_{n-1}} G_{\alpha'\alpha_1}(t, t') G_{\alpha_1\alpha_2}(t, t') \cdots G_{\alpha_{n-1}\alpha}(t, t'). \tag{A.9d}$$

Furthermore, by definition, the steady-state electronic transition probability for the scattering of an electron from a state α to a state α' is given by

$$W_{\alpha'\alpha} = \lim_{t-t' \to +\infty} \frac{\partial |P_{\alpha,\alpha}(t, t')|^2}{\partial (t - t')}. \tag{A.10}$$

In particular, the first-order contribution to the steady-state electronic transition rate is

$$W^{(1)}_{\alpha'\alpha} = \frac{1}{\hbar^2} \lim_{t-t' \to +\infty} \frac{\partial G^*_{\alpha'\alpha}(t, t') G_{\alpha'\alpha}(t, t')}{\partial (t - t')}. \tag{A.11}$$

References

[1] For early work, see, for example, Maan J C, Englert Th, Tsui D C and Gossard A C 1982 *Appl. Phys. Lett.* **40** 609

[2] Kawano Y, Hisanaga Y, Takenouchi H and Komiyama S 2001 *J. Appl. Phys.* **89** 4037

[3] Kawaguchi Y, Hirakawa K, Saeki M, Yamanaka K and Komiyama S 2002 *Appl. Phys. Lett.* **80** 136

[4] Kalugin N G, Nachtwci G, Vasilyev Yu B, Suchalkin S D and Eberl K 2002 *Appl. Phys. Lett.* **81** 382

[5] Hirakawa K, Yamanaka K, Kawaguchi Y, Endo M and Saeki M 2001 *Phys. Rev.* B **63** 85320

[6] For the case of $B = 0$, see, for example, Asmar N G, Markelz A G, Gwinn E G, Gerne J, Sherwin M S, Campman K L, Hopkins P E and Gossard A C 1995 *Phys. Rev.* B **51** 18041
Langerak C J G M, Murdin B N, Cole B E, Chamberlain J M, Henini M, Pate M and Hill G 1995 *Appl. Phys. Lett.* **67** 3453
Nordstrom K B, Johnsen K, Allen S J, Jauho A P, Birnir B, Kono J, Noda T, Akiyama H and Sakaki H 1998 *Phys. Rev. Lett.* **81** 457

[7] For the case of $B \neq 0$, see, for example, Heiss W, Auer P, Gornik E, Pidgeon C R, Langerak C J G M, Murdin B N, Weimann G and Heiblum M 1996 *Appl. Phys. Lett.* **67** 1110
Vaughan T A, Nicholas R J, Langerak C J G M, Murdin B N, Pidgeon C R, Mason N J and Walker P J 1996 *Phys. Rev.* B **53** 16481
Murdin B N, Hollingworth A R, Kamal-Saadi M, Kotitschke R T, Ciesla C M, Pidgeon C R, Findlay P C, Pellemans H P M, Langerak C J G M, Rowe A C, Stradling R A and Gornik E 1999 *Phys. Rev.* B **59** R7817

[8] For the recent development of FELs, see, for example, Feldhaus J and Weise H 2000 *Free Electron Laser 1999* (Amsterdam: Elsevier)

[9] For a review, see, for example, Xu W, Peeters F M, Devreese J T, Leadley D R and Nicholas R J 1996 *Int. J. Mod. Phys.* B **10** 169

[10] For optical measurements, see, for example, Wang Y J, Nickel H A, McCombe B D, Peeters F M, Shi J M, Hai G Q, Wu X-G, Eustis T J and Schaff W 1997 *Phys. Rev. Lett.* **79** 3226
[11] See, for example, Nicholas R J 1991 *Landau Level Spectroscopy* ed G Landwehr and E I Rashba (Amsterdam: Elsevier) p 777
[12] Xu W and Lin L B 2001 *J. Phys.: Condens. Matter* **13** 10889
[13] Ando T, Fowler A B and Stern F 1982 *Rev. Mod. Phys.* **54** 437
[14] Meyer B K, Hofmann D M, Volm D, Chen W M, Son N T and Janzén E 2000 *Phys. Rev.* B **61** 4844
[15] See, for example, Messiah A 1970 *Quantum Mechanics* vol 2 (Amsterdam: North-Holland)
[16] See, for example, Mattuck R D 1976 *A Guide to Feynman Diagrams in the Many-Body Problem* (New York: McGraw-Hill)